Aerosol and Air Quality Research, 17: 278–289, 2017

ISSN: 1680-8584 print / 2071-1409 online
doi: 10.4209/aaqr.2016.06.0271

Backward Integration of Diffusion Equation

Wen-Yih Sun[1,2,3*], Oliver M. Sun[4]

[1] *Department of Earth, Atmospheric and Planetary Sciences, Purdue University, W. Lafayette, IN 47907, USA*
[2] *Department of Atmospheric Sciences, National Central University, Zhongli, Taoyuan City 32001, Taiwan*
[3] *Hydrospheric Atmospheric Research Center (HyARC), Nagoya University, Nagoya 464-8601, Japan*
[4] *Naval Undersea Warfare Center, Newport, RI 02841-1708, USA*

ABSTRACT

When the parabolic differential equation is integrated backward in time, it can create unwanted shortwaves with large amplitude. Hence, instead of solving it as a differential equation, the diffusion equation is converted to the equations of volume-integrated-concentration, and mixing/diffusion is treated as subgrid-turbulent-fluxes across the cell boundaries. Those equations become a set of linear algebra equations and can be solved in both forward- and backward-in time. The proposed method has been validated by the numerical simulations of an idealized case, which consists of 5 different sizes of concentric cylinders with different species. The time evolution of compositions shows that the concentrations in each cylinder can change drastically with time. For the data collected at downwind region, the proposed reverse-in-time integration can be used to assess the concentrations at the source regions, which can be quite different from those derived from the conventional backward-trajectory method without mixing. It also shows that the traditional forward-trajectory or backward-trajectory method without mixing (i.e., Lagrangian method) widely used in meteorology and air pollution can misinterpret the property of fluid parcel at both upwind and downwind regions significantly.

Keyword: Forward and backward integration; Diffusion; Parabolic and hyperbolic equations; Mixing/Diffusion-time scale; Turbulence; Pollution.

INTRODUCTION

Turbulent mixing and diffusion are important in fluid dynamics. It has been included in most atmospheric and ocean models to simulate/predict weather, climate, and oceanic phenomena. Numerical models are also applied to study the transport and dispersion of aerosols and pollutants in the atmosphere and oceans. The advection-diffusion equations in those models are usually integrated forward-in-time, starting from the source as an initial condition to simulate the transport and dispersion of the plumes or thermal as time increases (Sun, 1989; Sun *et al.*, 2013a, b). From the concentrations in the downwind region, backward-trajectory-method (Choi *et al.*, 2001) is frequently used to estimate the property of the parcel at source derived from backward advection equations without mixing, because the reverse diffusion can easily become unstable for short-wave perturbations. It is also noted that Cauchy problem for the reverse heat (diffusion) equation ($\partial u/\partial t = a\partial^2 u/\partial^2 x$, wih $a < 0$) is incorrect in the sense that it does not have continuous dependence of the solution on the initial function (Lavrentiev *et al.*, 1980). Small errors of the data lead to a large errors in the results. It is necessary to filter out all information containing higher Fourier coefficients (Engl *et al.*, 2000). Hence, Scientists have proposed "Regularization" by introducing addition information in order to solve this ill-posed problem. For example, Sikora and Palka (1980) proposed a method consisting of solving the Volterra integral equation of the first kind by means of Tikhonov regularization method. This approach requires complicated mathematics and computation, which may not be applicable to the real pollution problems.

It is also noted that the standard linear parabolic models based on Fourier's law (1822) or Fick's law (1855) predict an infinite speed of propagation, which may violate physics. Hence, Cattaneo (1958), Vernotte (1958), Chester (1963), and others proposed that Fourier equation should be upgraded from the parabolic to a hyperbolic form,

$$\frac{1}{\alpha^2}\frac{\partial^2 \mathrm{C}}{\partial \mathrm{t}^2}+\frac{1}{\kappa}\frac{\partial \mathrm{C}}{\partial \mathrm{t}}=\nabla^2 \mathrm{C},$$

where α is called the speed of second sound. Then, the equation can be solved as waves, which can propagate forward and backward. However, the solutions are sensitive

* Corresponding author.
E-mail address: wysun@purdue.edu

to the relaxation time ($\tau_r = \kappa/\alpha^2$) and may become complex numbers. The solution may be acceptable according to the second law of thermodynamics, it seems unrealistic for gaseous material and possibly for most solids (Taiel, 1971). Hence, forward-in-time integration was applied in most traditional diffusion equations (Sun, 1982).

As shown in Sun and Chang (1986) and Sun (1988, 1989), the change of concentration C can be rewritten as:

$$\frac{\partial C}{\partial t} + V \bullet \nabla C = \nabla \bullet k \nabla C \tag{1a}$$

or

$$\frac{\partial C}{\partial t} + V \bullet \nabla C = -\nabla \bullet (\overline{C'V'}) \tag{1b}$$

where V is the velocity, and $\overline{C'V'}$ is the subgrid-turbulent flux of C. We can integrate (1b) over any specific cell if the turbulent flux around the boundaries can be formulated properly. Hence, we can convert (1a) from a differential equation into equations of volume-integrated-concentration, which can be integrated forward or backward in time. The proposed method can avoid creating undesirable shortwaves, because the size of the cells are well defined. If there is no internal source or sink, according to conservation of mass, the change of mass in each cell is equal to the net mass fluxes across the boundaries, consisting of cell- and subgrid-scale fluxes. The diffusion process can be interpreted as the subgrid-flux, which depends on density perturbations and the turbulent kinetic energy (TKE) at the boundaries. For simplicity, it is assumed that size of each cell is time independent and density inside each cell is uniformly distributed, then, we can easily convert the integration equations to a set of linear algebra equations, which depend on the size of cells, concentration, and the turbulent velocity. The method can be modified and applied to the cases that containers, wind, and turbulences are function of time. The numerical results for the idealized cases are quite accurate if integration is comparable or less than the diffusion-time-scale, τ, which is a function of volume (V) and TKE. If integration is longer than diffusion-time, majority of the original material in the individual cell is replaced by the substances of the surroundings in the forward-in-time integration. It is also noted that the error increases as the reverse-integration time increases.

Severe air pollution usually occurs when the atmosphere is very stable with little mixing, under such condition we can obtain highly accurate results after a long backward-in-time integration. If the atmospheric stratification is near neutral with strong mixing, pollutants can disperse quickly, and air quality may become more tolerable, under this condition we cannot perform a long reverse-integration without introducing significant errors, because the time scale of backward-integration is limited by the mixing/diffusion-time-scale. Since the property of the air parcel at the downwind regions can be significantly different from that at the source regions. Hence, the traditional forward-backward trajectory method without including mixing is valid only when the time scale is much shorter than the diffusion-time-scale τ, which will be defined later.

EQUATION AND NUMERICAL MODEL

According to Leibniz' rule, the change of density $\rho_m^j = \overline{\rho_m^j}$(cell-sized mean)+$\rho_m^{j'}$(perturbation) for the m^{th} specie in the j^{th} cell with velocity $V^j = \overline{V^j}$(cell-sized mean)+ V^{j}'(perturbation) are:

$$\begin{aligned}
&\frac{D}{Dt}\int_{V_j}\rho_m^j dV = \int_{V_j}\frac{\partial \rho_m^j}{\partial t}dV + \oint \rho_m^j V^j \bullet n dA = -\int_{V_j}\rho_m^j S_m^j dV,\\
&\int_{V_j}\frac{\partial \overline{\rho_m^j}}{\partial t}dV + \oint \overline{\left(\overline{\rho_m^j}+\rho_m^{j'}\right)\left(\overline{V^j}+V^{j}'\right)} \bullet n dA = -\int_{V_j}\overline{\rho_m^j} S_m^j dV,\\
&\int_{V_j}\frac{\partial \overline{\rho_m^j}}{\partial t}dV + \oint \overline{\rho_m^j}\,\overline{V^j} \bullet n dA + \oint \overline{\rho_m^{j'} V^j}' \bullet n dA = -\int_{V_j}\overline{\rho_m^j} S_m^j dV,\\
&\int_{V_j}\frac{\partial \overline{\rho_m^j}}{\partial t}dV + \int_{V_j}\nabla \bullet \left(\overline{\rho_m^j}\,\overline{V^j}\right)dV = -\oint \overline{\rho_m^{j'} V^j}' \bullet n dA - \int_{V_j}\overline{\rho_m^j} S_m^j dV,\\
&\int_{V_j}\frac{D\overline{\rho_m^j}}{Dt}dV + \int_{V_j}\overline{\rho_m^j}\nabla \bullet \overline{V^j} dV = -\oint \overline{\rho_m^{j'} V^j}' \bullet n dA - \int_{V_j}\overline{\rho_m^j} S_m^j dV.
\end{aligned} \tag{2}$$

where $\rho_m^j S_m^j$ is the sink of ρ_m^j, it is also assumed that $\nabla \bullet \overline{V^j} = 0$ and sizes of the cells remain constant. The bar of cell-sized mean will be dropped hereafter. Following the Lagrangian frame, the change of the mass $\int_{V_j}\frac{D\rho_m^j}{Dt}dV$ with density ρ_m^j for the m^{th} specie in the j^{th} cell with time-independent volume V_j can be given by:

$$\frac{D\rho_m^j}{Dt} = \frac{1}{V_j}\left\{-\rho_m^j \sum_{i\neq j} A_{i,j} u_{i,j}^{'} + \sum_{i\neq j}\rho_m^i A_{i,j} u_{i,j}^{'} - \rho_m^j V_j S_m^j\right\} \tag{3}$$

for i = 1, 2, .., J; j = 1, 2, .., J; and m = 1, 2, .., M

where A_{ij} is the surface area between the i^{th} and j^{th} cells, and $u_{i,j}^{'}$ is the turbulent velocity on A_{ij}. The terms on the right hand side indicate the material of m^{th} specie getting out from j^{th} cell, getting into j^{th} cell from outside, and the internal sink inside j^{th} cell, respectively. For simplicity, V_j, $A_{i,j}$, and $u_{i,j}^{'}$ are time-independent in this study. Otherwise, Eq. (2) should be applied. The finite difference form of Eq. (3) becomes

$$\begin{aligned}
\frac{\left(\rho_m^j\right)^{n+1}-\left(\rho_m^j\right)^n}{\Delta t} = \frac{1}{V_j}\Bigg\{&-\left[p\left(\rho_m^j\right)^n + q\left(\rho_m^j\right)^{n+1}\right]\sum_{i\neq j}A_{i,j}u_{i,j}^{'}\\
&+\sum_{i\neq j}\left[p\left(\rho_m^i\right)^n + q\left(\rho_m^i\right)^{n+1}\right]A_{i,j}u_{i,j}^{'}\\
&+\left[p\left(\rho_m^j\right)^n + q\left(\rho_m^j\right)^{n+1}\right]V_j S_m^j\Bigg\}
\end{aligned}$$

for j = 1, 2, .., J; i = 1, 2, .., J; and m = 1, 2, .., M (4)

An implicit-time step is applied on the right hand, where q = 1 – p, and 0 ≤ p ≤ 1. (4) Becomes:

$$\left(\rho_m^j\right)^{n+1}\left\{1+q\left[\sum_{i\neq j}\left(\frac{A_{i,j}}{V_j}\right)u_{i,j}^{'}\Delta t+S_m^j\right]\right\}$$
$$-q\sum_{i\neq j}\left(\frac{A_{i,j}}{V_j}\right)u_{i,j}^{'}\Delta t\left(\rho_m^i\right)^{n+1}=$$
$$\left(\rho_m^j\right)^{n}\left\{1-p\left[\sum_{i\neq j}\left(\frac{A_{i,j}}{V_j}\right)u_{i,j}^{'}\Delta t+S_m^j\right]\right\} \quad (5)$$
$$+p\sum_{i\neq j}\left(\frac{A_{i,j}}{V_j}\right)u_{i,j}^{'}\Delta t\left(\rho_m^i\right)^{n}$$

for j = 1, .., J; i = 1, .., J; and m = 1, .., M

We assume that p = 0.5 in order to have the 2nd order accuracy in time. Eq. (5) can be solved by LU-method for the forward-in-time from an initial condition to study the dispersion of species as time increases. It can also be solved for the reverse-in-time from the concentrations collected from the downwind regions to assess the initial conditions and time evolution between the time intervals.

The model consists of two layers of cylinders as shown in Fig. 1. The mean height of the PBL is somewhere between 1 km to 2 km (Medeiros *et al.*, 2005), but it may be higher over the industrial and urban areas, so we set it as 2000 m for the depth of the lower layer, which is topped by the cylinder E (light yellow) with radius of 30,000 m and thickness of 2,222.2 m, in the lower part of the free atmosphere above the PBL. The lower layer consists of 4 concentric cylinders: A (black), B (red), C (green), and D (blue), with radii of R_{AB} (between cylinders A and B) = 5,000 m, R_{BC} (between cylinders B and C) = 10,000 m, R_{CD} (between cylinders C and D) = 20,000 m, and R_D (outside of D) = 30,000 m. The volume is 157,079 × 10^6 m^3 for cylinder A; 471,239 × 10^6 m^3 for cylinder B; 188,496 × 10^7 m^3 for cylinder C; 314,159 × 10^7 m^3 for cylinder D; and 628,256 × 10^7 m^3 for cylinder E. Different species with uniform density are assigned to different cylinders initially. The turbulent velocity u' between two neighbor volumes should be proportional to the TKE, which can be obtained from observations or numerical models but is not calculated in this study. Hence, an assigned value of TKE is used here. It is noted that the TKE was explicitly calculated in many atmospheric models, including Purdue Regional Climate Model (Sun and Chern, 1993; Sun *et al.*, 2009; Min and Sun, 2015) and NTU-Purdue Model (Hsu and Sun, 2001, Sun and Sun, 2015), and CRESS model (Tsuboki and Sakakibara, 2007; Sun *et al.*, 2012, 2013c), etc.

Severe pollutions usually occur in a calm, stable condition. Observations showed that for the weak-wind (< 5 m s^{-1} in the lowest 200 m), very stable boundary layer (with Richardson Number ≥ 0.6). The boundary layer was very shallow (sometime < 10 m deep), and turbulent fluxes between the earth's surface and the atmosphere were found to be essentially shut down with TKE being near zero (Banta, 2008). The PBL above this strong surface inversion may be still quite stable, hence, the value of horizontal u' is set to 2.5 × 10^{-2} m s^{-1}. The vertical mixing u' between the cylinder E in the upper layer and those in the lower layer is set equal to 0.1 of the horizontal u' in the lower layer, because vertical mixing is suppressed under the stable stratification. Since step functions are applied to ρ_m^j, density perturbation across the cells' boundary, $\rho_m^{j'}$, should be much larger than that with a continuous-variation of density among different cells. Since flux at the boundary is determined by $u'\rho'$, a smaller value of u' may compensate a larger value of ρ' applied in the study. Different value of u' will also be discussed later. The time interval Δt = 50 s is applied to both the forward and reverse integrations. It is noted this method proposed here can be modified and applied to the cases when u' and the size of cylinders change with time according to (2).

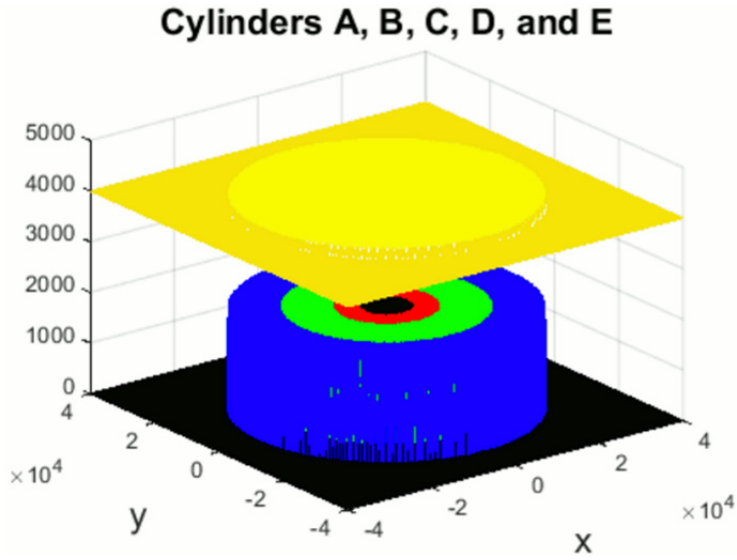

Fig. 1. The size and arrangement of cylinders in this study.

NUMERICAL RESULTS

Forward-in-Time Integration

In order to simplify tracing the dispersion of the material with time, each cylinder has its unique specie with one unit amount of density initially, as shown in Table 1. It is also assumed that the specie will maintain its identity during integration. The time evolutions of the density of species in each cylinder are shown in Figs. 2(a)–2(e). The black color indicates the material originally in cylinder A; red in cylinder B; green in cylinder C; blue in cylinder D; and light blue in the upper cylinder E. Initially, ρ_1^A (specie 1 in cylinder A, black line) decreases with time exponentially, which is replaced by the material coming from cylinders B (ρ_2^A specie 2 in cylinder A, red line), C (ρ_3^A green), D (ρ_4^A in blue), and E (ρ_5^A in light blue). The density of those invaders starts from zero and increases with time as shown in Fig. 2(a). The decrease of ρ_1^A slows down as time increases, because amount of $\rho_1{}^A$ decreases with time. $\rho_1^A = \rho_2^A \cong 0.35$ at $t = 1.1 \times 10^5$ s; $\rho_1^A = \rho_3^A \cong 0.23$ at $t = 1.7 \times 10^5$ s; at the end of integration, t (= tf) = 4×10^5 s (~111.1 hrs.), $\rho_1^A \cong 0.07$, while $\rho_2^A = 0.144$, $\rho_3^A = 0.26$, $\rho_4^A = 0.20$, and $\rho_5^A = 0.32$ as shown in Table 1 and Fig. 2(a). The concentration of $\rho_1^A \cong 0.2$ at $t = 2 \times 10^5$ s shows that most of original material is replaced by the substances from outside by this time, especially those with vast volumes, only 7% of the original material remains at $t = 4 \times 10^5$ s. On the other hand, the concentration of A at tf in the downwind will be interpreted as that of A initially according to the backward-trajectory method. Because of diffusion, the material of each cell in the downwind is quite different from the original source. Hence in meteorology and other fields,

Table 1. Initial value of ρ_m^k.

ρ_m^k	m = 1	m = 2	m = 3	m = 4	m = 5
k = A	1.0	0.0	0.0	0.0	0.0
k = B	0.0	1.0	0.0	0.0	0.0
k = C	0.0	0.0	1.0	0.0	0.0
k = D	0.0	0.0	0.0	1.0	0.0
k = E	0.0	0.0	0.0	0.0	1.0
Total mass (M_0)	1.571×10^{11}	4.712×10^{11}	1.885×10^{12}	3.142×10^{12}	6.283×10^{12}

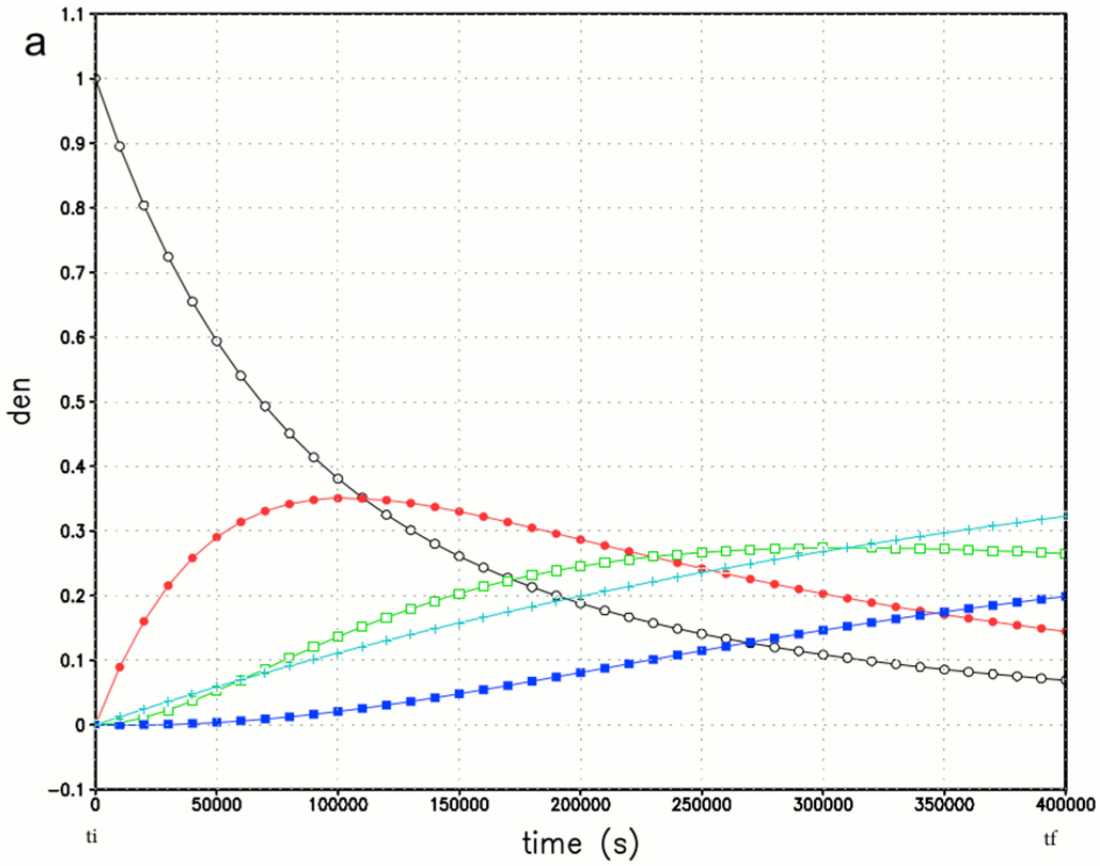

Fig. 2. Different species at each cell: (a) $\rho_1^A, \rho_2^A, \rho_3^A, \rho_4^A$, and ρ_5^A; (b) $\rho_1^B, \rho_2^B, \rho_3^B, \rho_4^B$, and ρ_5^B; (c) $\rho_1^C, \rho_2^C, \rho_3^C, \rho_4^C$, and ρ_5^C; (d) $\rho_1^D, \rho_2^D, \rho_3^D, \rho_4^D$, and ρ_5^D; (e) $\rho_1^E, \rho_2^E, \rho_3^E, \rho_4^E$, and ρ_5^E.

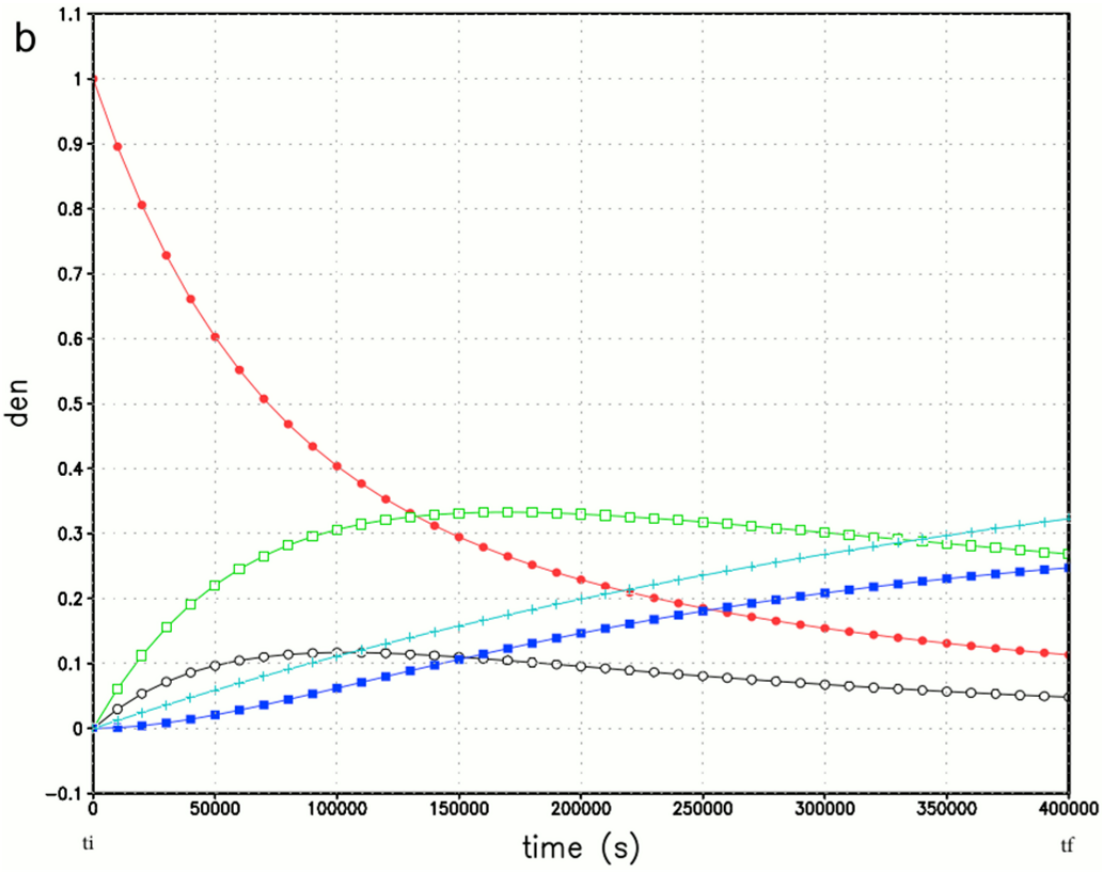

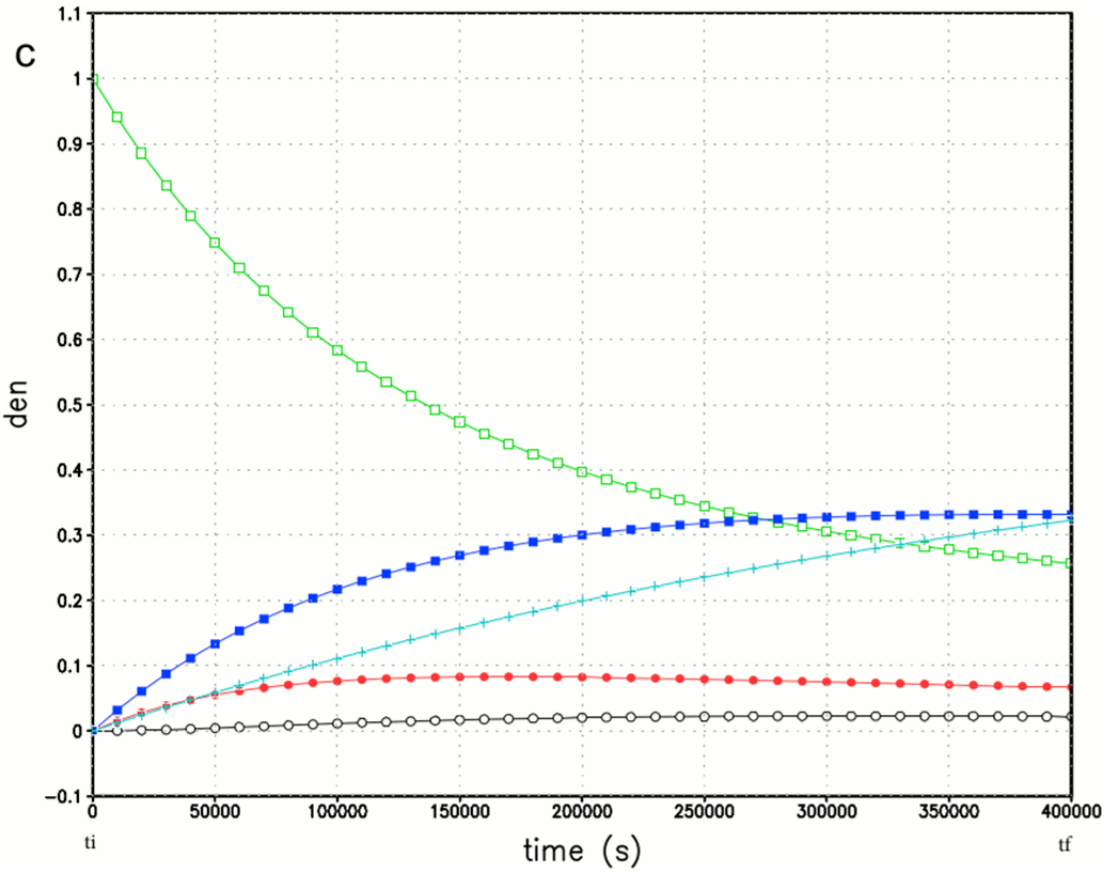

Fig. 2. (*continued*).

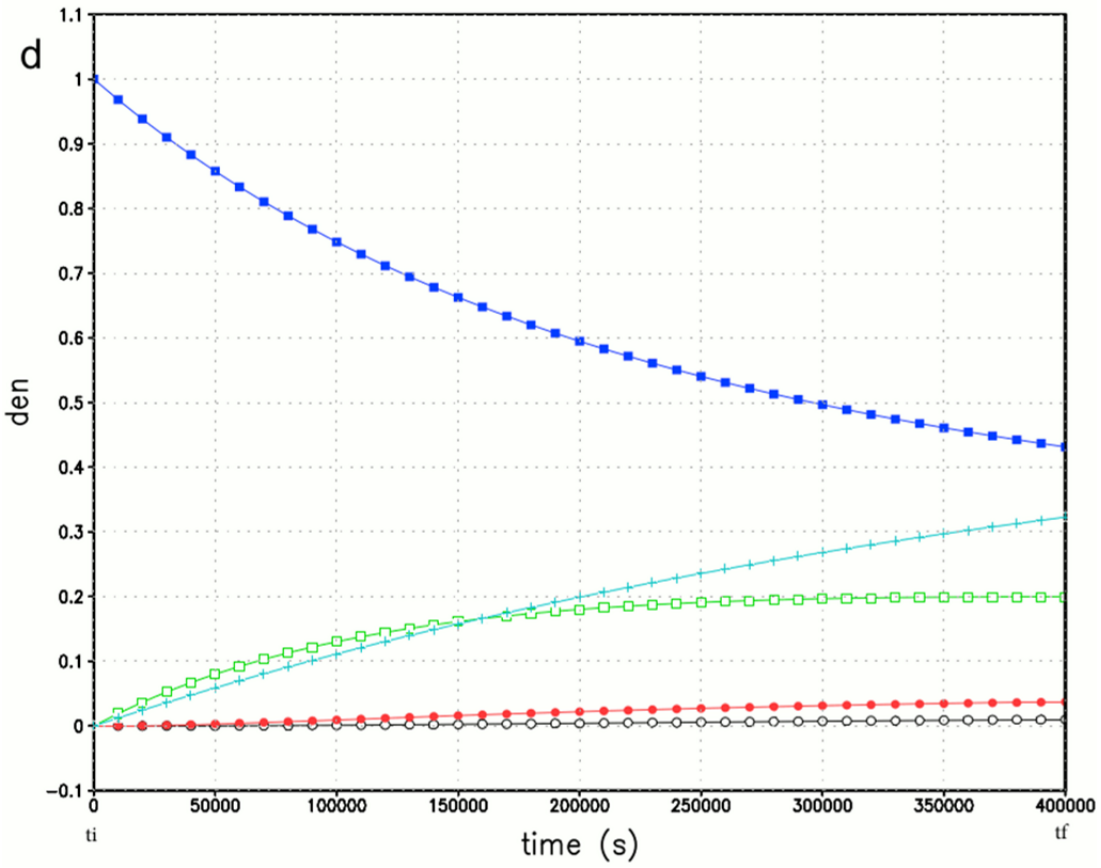

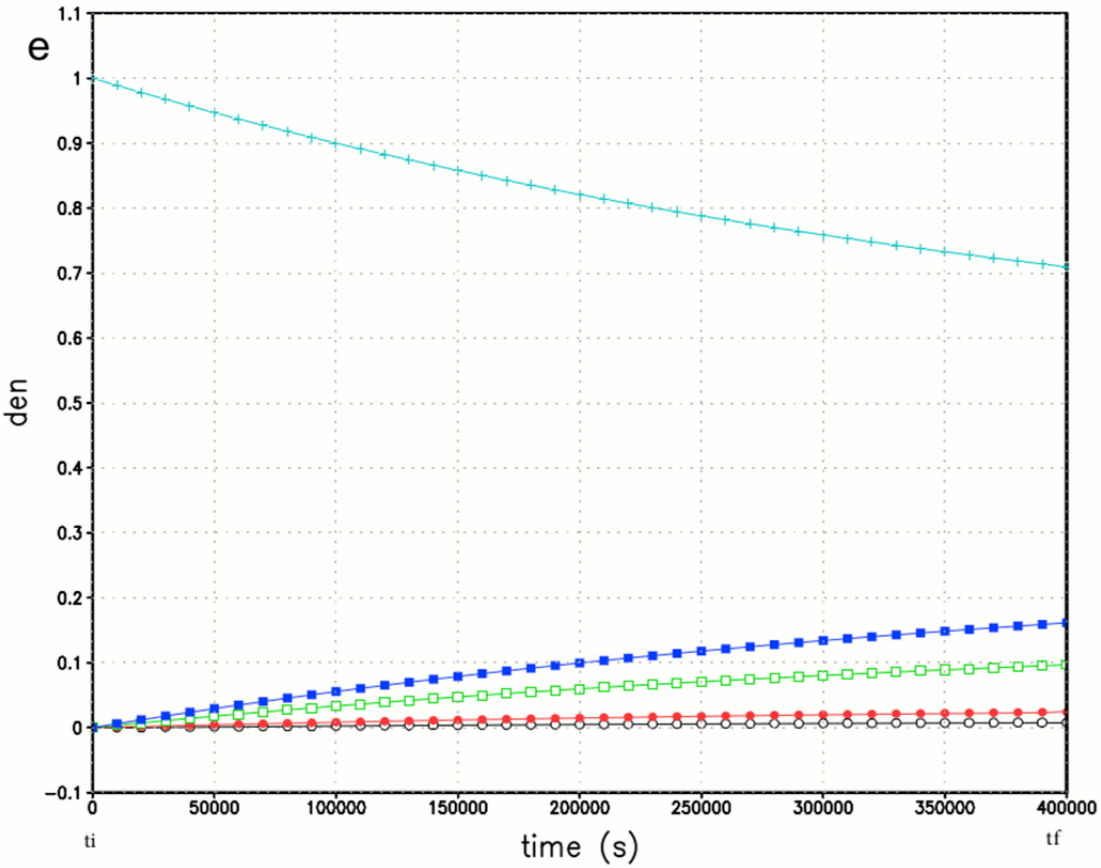

Fig. 2. (*continued*).

the conventional forward- or backward-trajectory-method can lead to a significant error to interpret the property, because it ignores mixing with the surroundings.

The distribution of ρ_2^B (species 2 in cylinder B), shown in Fig. 2(b), is very similar to ρ_1^A in Fig. 2(a). ρ_3^B in Fig. 2(b) is also similar to ρ_2^A in Fig. 2(a). Because of relatively small volume of cylinder B, the original material is quickly replaced by the material coming from other cylinders. Only about 23% of the original ρ_2^B still retains at $t = 2 \times 10^5$ s, and only about 11% remains at $t = tf = 4 \times 10^5$ s.

Figs. 2(c)–2(e) show that the larger the volume, the more the original material can be retained. It is also noted that Cylinder E (Fig. 2(e)) can keep up more than 70% of the original material because of large volume as well as a small u' between Cylinder E and the cylinders in the lower layer. Fig. 2(e) also shows that the contributions from the lower cylinders are proportionally to their contact-areas with Cylinder E. The initial density and total amount of each specie in those five cylinders are shown in Table 1.

The time variations of each specie among different cylinders, which are indicated by black (in cylinder A), red (B), green (C), blue (D), and light blue (E) lines marked with plus (+) are shown in Figs. 3(a)–3(e). As discussed previously, at $t = 4 \times 10^5$ s, most of the original material in cylinder A is replaced by the material from outside, only 7% remains (ρ_1^A = 0.069 (black)), which is slighter higher than specie 1 in other cells, ρ_1^B (= 0.048 (red)) and ρ_1^C (= 0.022 (green)) as shown in Fig. 3(a). On the other hand, ρ_2^A (= 0.14 (black)) is higher than ρ_2^B (= 0.11 (red)) shown in Fig. 3(b) and Table 2; ρ_3^A (= 0.265 (black)) and ρ_3^B (= 0.268 (red)) are slightly higher than ρ_3^C (= 0.256 (green)) as shown in Fig. 3(c) and Table 2, although the mass of $m_3^C = V_c \bullet \rho_3^C$ is still larger than that of $m_3^A = V_A \bullet \rho_3^A$ or $m_3^B = V_B \bullet \rho_3^B$. Because $(A_{5,j} / V_j) u'_{5,j} = u'_{5,j} / H_L$, (where H_L is the depth of lower cylinders), is same for each lower cylinder, the increase of $\rho_5^A, \rho_5^B, \rho_5^C$, and ρ_5^D are also the same, although the mass increment of each cylinder depends on the volume of cylinder.

Reverse-in-Time Integration

Using the density distribution of each specie at $t = 4 \times 10^5$ s shown in Table 2 as initial condition, we integrate Eq. (5) reverse-in-time, i.e., we calculate $(\rho_m^j)^n$ from a given $(\rho_{pn}^j)^{n+1}$ by Eq. (5). The integrated density from $t = tf = 4 \times 10^5$ s to the end at $t = ti = 0$ are shown in Figs. 3(a)–3(e) for species 1 to 5, which are indicated by black, red, green, blue, and light blue lines marked with "○" signs.

Figs. 3(a)–3(e) show that the reverse-in-time integrations (with ○) coincide the track of the forward-in-time integrations (with +). The results end up almost identical to the initial condition used in the forward-in-time integration. ρ_5^A (Fig. 3(e)) has an error of 1.15% after 8,000 times of forward-

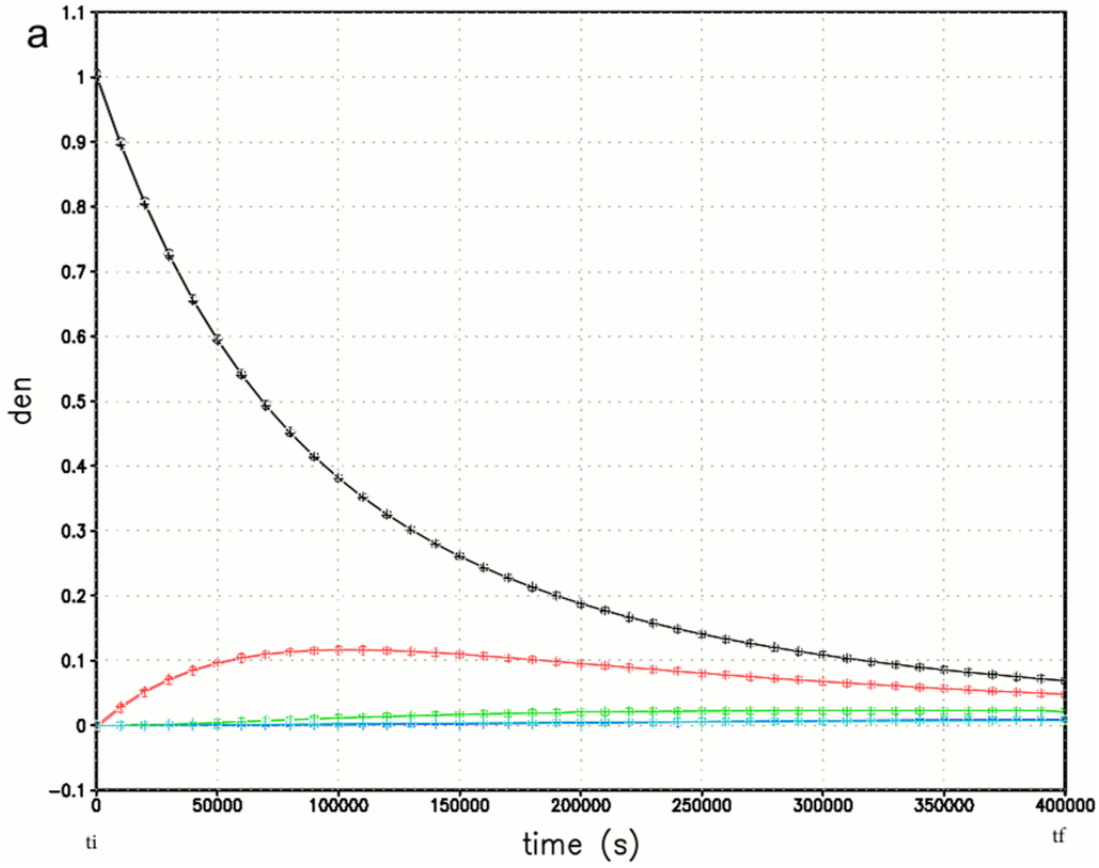

Fig. 3. Forward-integrations + and backward-integrations ○ for species among different cells: (a) $\rho_1^A, \rho_1^B, \rho_1^C, \rho_1^D$, and ρ_1^E; (b) $\rho_2^A, \rho_2^B, \rho_2^C, \rho_2^D$, and ρ_2^E; (c) $\rho_3^A, \rho_3^B, \rho_3^C, \rho_3^D$, and ρ_3^E; (d) $\rho_4^A, \rho_4^B, \rho_4^C, \rho_4^D$, and ρ_4^E; (e) $\rho_5^A, \rho_5^B, \rho_5^C, \rho_5^D$, and ρ_5^E.

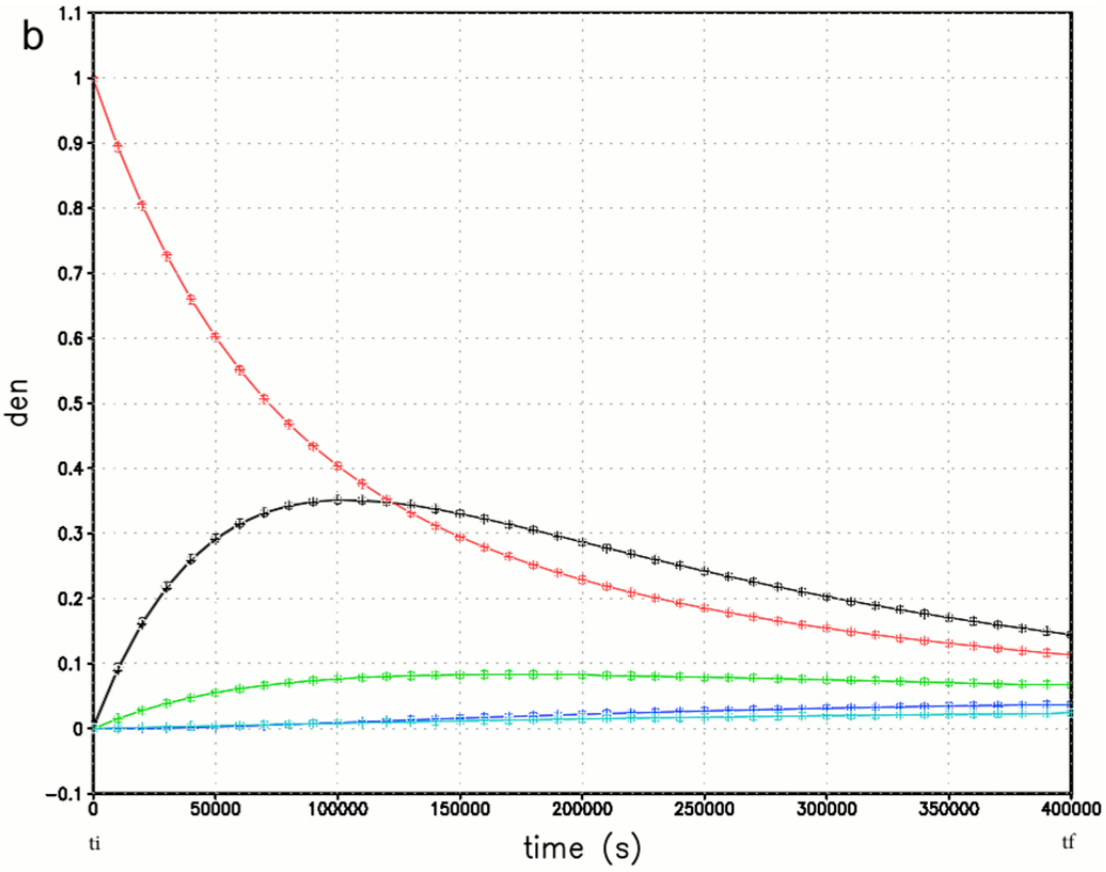

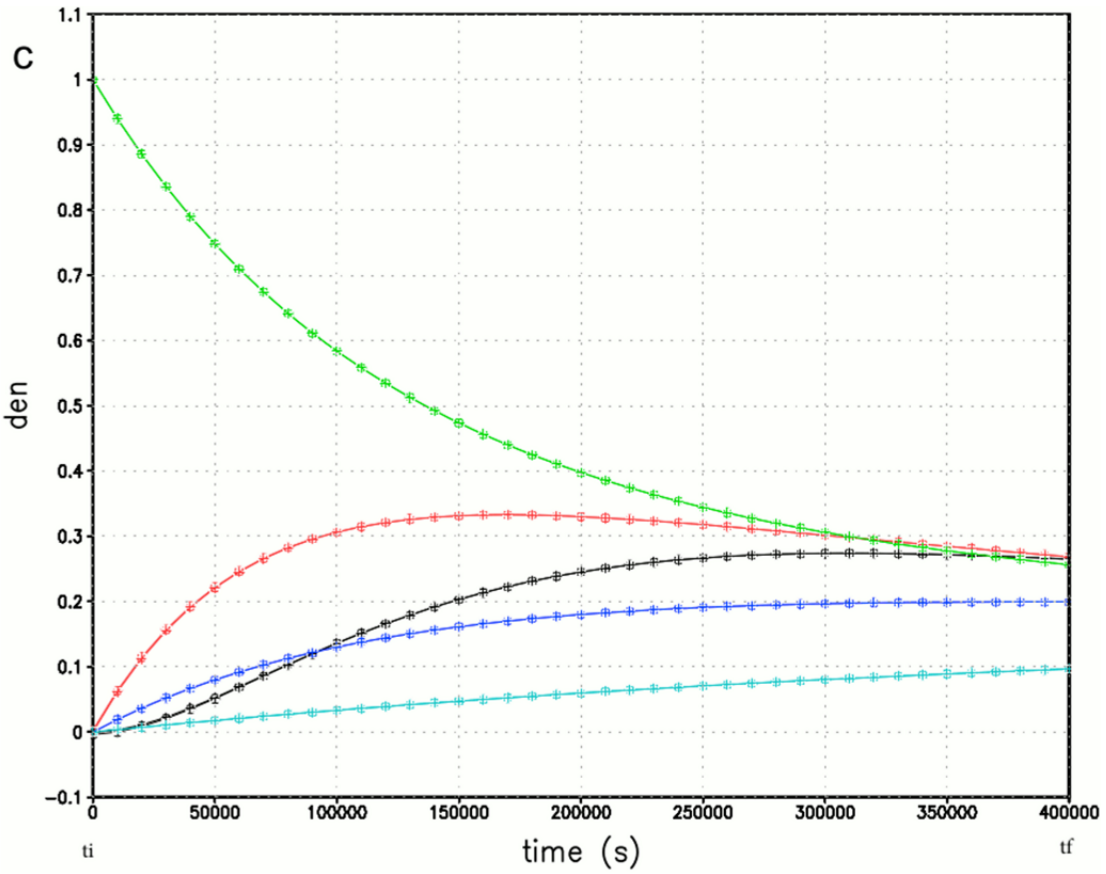

Fig. 3. (*continued*).

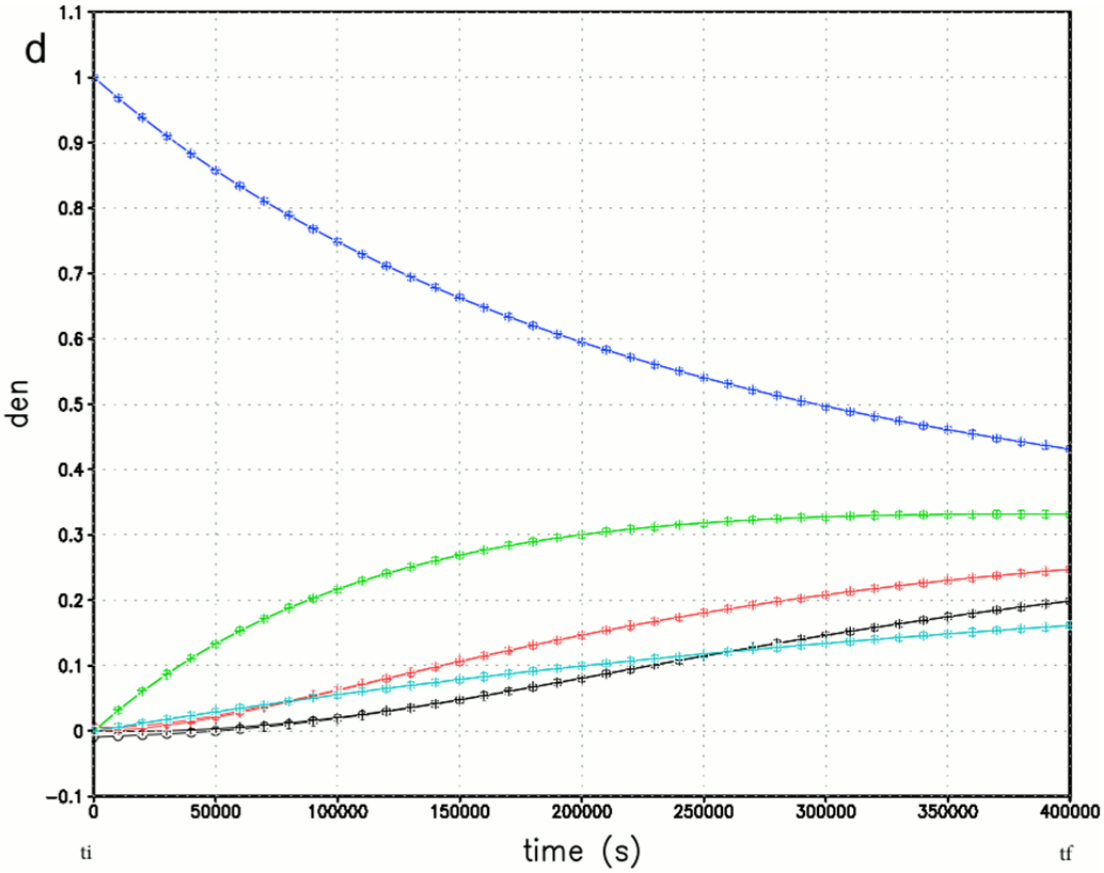

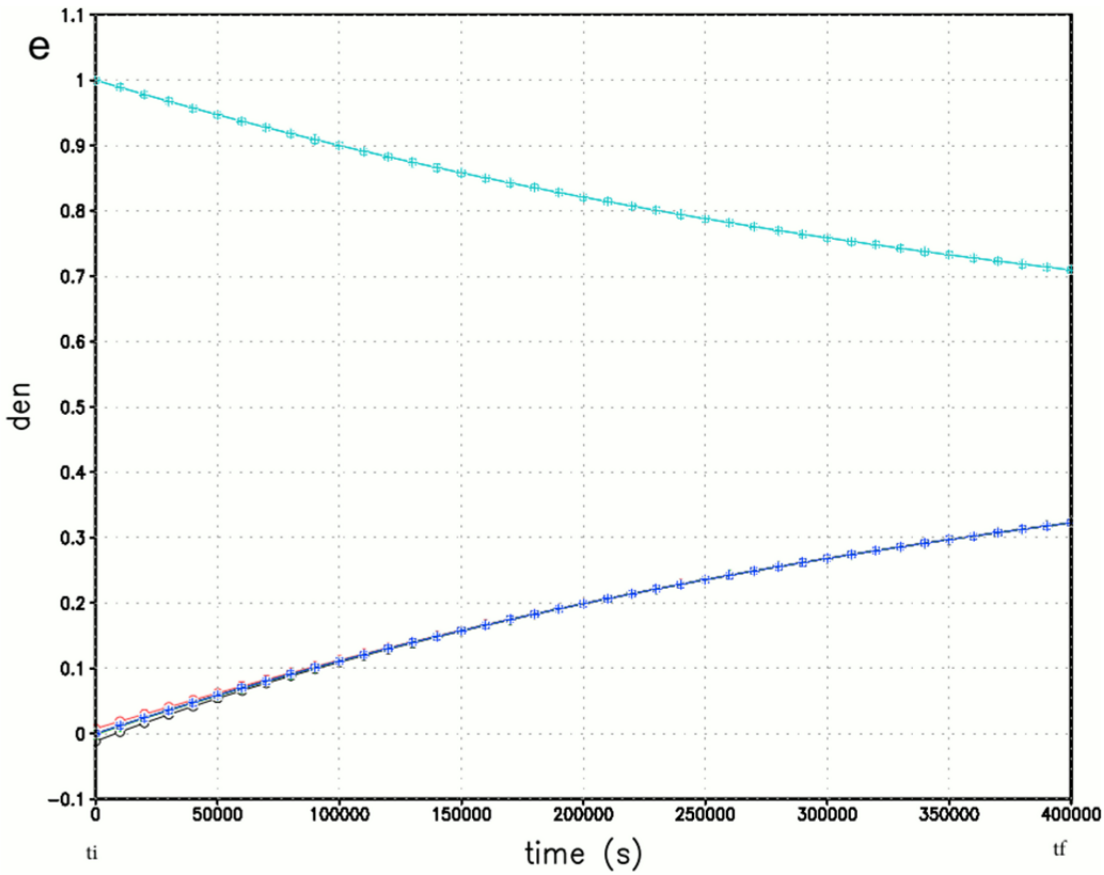

Fig. 3. (*continued*).

Table 2. Value of ρ_m^k at t = 4×10^5 s (~111.1 hrs) from forward integration.

ρ_m^k	m = 1	m = 2	m = 3	m = 4	m = 5
k = A	$0.6905993479 \times 10^{-1}$	0.1445150903	0.2647582919	0.1988422684	0.3227885866
k = B	$0.4814514006 \times 10^{-1}$	0.1131864438	0.2684946612	0.2473345404	0.3227908228
k = C	$0.2203935670 \times 10^{-1}$	$0.6708729338 \times 10^{-1}$	0.2563843611	0.3316312765	0.3227804744
k = D	$0.9929036647 \times 10^{-2}$	$0.3706982920 \times 10^{-1}$	0.1989195485	0.4312301019	0.3227838843
k = E	$0.8061160947 \times 10^{-2}$	$0.2419257409 \times 10^{-1}$	$0.9680327115 \times 10^{-1}$	0.1613735110	0.7095206872
Total mass (M_{end})	1.569×10^{11}	4.710×10^{11}	1.885×10^{12}	3.142×10^{12}	6.283×10^{12}
$(M_{end} - M_0)/M_0$	-1.005×10^{-3}	-5.928×10^{-4}	-2.186×10^{-4}	-1.815×10^{-6}	2.579×10^{-5}

integration plus same number of reverse-integration. Fig. 3(b) shows that ρ_2^A (= 0.145) is larger than ρ_2^B (= 0.113) at tf = 4×10^5 s, but at the end of the reverse-integration $\rho_2^A = 0$ and $\rho_2^B = 1$. The values of ρ_3^A, ρ_3^B, and ρ_3^C are around 0.26 at tf = 4×10^5 s, after the reverse-integration $\rho_3^A = \rho_3^B = 0$ and $\rho_3^C = 1$ at t = 0. It indicates that the reverse-integration can handle the counter-gradient flux, which is difficult to simulate in the diffusion equation even in the forward-in-time calculation (Sun and Chang, 1986; Sun, 1988, 1989).

The simulations show the importance of mixing among the cells. Because of mixing, the material at the downwind region can be significantly different from its original source, which cannot be derived from the forward-trajectory method without mixing. Meanwhile, it is impossible to predict the property at the sources from the downwind regions using the conventional backward-trajectory-method. Both forward-trajectory and backward-trajectory methods without mixing are referred as the Lagrangian method and have been widely used in meteorology and air quality researches.

Here, we provide a different approach. From the observed concentrations at downwind and meteorological conditions, the proposed backward-in-time integration method can be applied to analyze the contributions coming from the source and surroundings in the upstream regions.

Time Scale of Mixing/Diffusion

Both forward- and reverse-in-time integrations, the solutions depend on

$$\left(\frac{A_{i,j}}{V_j}\right) u'_{i,j} n\Delta t \sim \frac{u'_{i,j} n\Delta t}{\left(V_j\right)^{1/3}} \sim \frac{u'_{i,j} t_n}{\left(V_j\right)^{1/3}} \sim \frac{u'_{i,j} t_n}{L_j} \sim \frac{t_n}{\tau_j} \tag{6}$$

where L_j is the length scale of the j^{th}-cell, τ_j, ($\tau_j \sim \frac{L_j}{u'_{i,j}} \sim \frac{\left(V_j\right)^{1/3}}{u'_{i,j}}$) is the time scale of mixing/diffusion for j-cell, and n is the number of time-step of integration. The time scale of mixing/diffusion $\tau_j \sim L_j/u' \sim 200{,}000$ s for Cylinder A, and $\tau_j \sim 600{,}000$ s for cylinder D. Table 3 shows that the error combining both forward- and backward-integrations decreases with the increase of cylinder size, as expected. The error for cylinder A is about 0.01, and 0.001 for cylinder C, both errors are associated with specie 5. The results are quite accurate if the integration time is order of τ_j or smaller. However, if the integration time is longer, the error may increase drastically.

If the size of cylinders remains constant, we can obtain the same results as long as $u'_{i,j} t_n$ does not change. Hence, the integration time t_n should be shorter if the turbulent velocity $u'_{i,j}$ is stronger in order to keep $t_n/\tau_j \leq 1$. On the other hand, t_n can be longer for weaker turbulence. For example, if the volume of cells remains the same. The results shown in Table 1, 2 and Figs. 2, 3 for the case with tf = 4×10^5 s and $u'_{1,2} = 2.5 \times 10^{-2}$ m s^{-1} are also applied to the cases with tf = 2×10^5 s and $u'_{1,2} = 5 \times 10^{-2}$ m s^{-1}; or tf = 6×10^5 s and $u'_{1,2} = 1.67 \times 10^{-2}$ m s^{-1}, etc. A larger value of $u'_{i,j}$ implies stronger mixing among the cylinders. The property of cylinders dilutes quicker, especially for the small-sized cylinders. On the other hand, a smaller value of $u'_{i,j}$ corresponds to weaker mixing, such that original elements can retain longer.

If the turbulent velocity keeps constant, the results remain the same when $\frac{t_n}{\left(V_j\right)^{1/3}} \sim \frac{t_n}{L_j}$ remains constant according to Eq. (6). It indicates with the same turbulent intensity, a small sized cell quickly mixes with surrounding and is more difficult to trace back from reverse integration. Hence, the results shown in Figs. 3(a)–3(e) and Table 3 are also valid for the cylinders with different sizes or different depth of PBL, as long as time-integration is adjusted to length scale accordingly (i.e., $\frac{t_n}{\left(V_j\right)^{1/3}} \sim \frac{t_n}{L_j} \sim$ constant). Hence, a long-time integration should be applied to the large-sized cells under weak turbulent condition. Since each specie remains its identity (i.e., without chemical reaction), the results obtained here can be applied to the case such that each cell has any different combinations of those species initially.

It is noted that wind, turbulent velocity and the size of cells in the real atmosphere and oceanography are time-dependent. Hence, the turbulent velocity and the volume of cells proposed here should be modified according to the atmospheric model simulations or observations. Similarly, sink/source term should include deposit and chemical reactions in order to simulate the transport and dispersion in the real atmosphere and oceans, as discussed in Sun *et al.* (2013a, b), and Yang (2004).

CONCLUSIONS

Backward integration of the parabolic equation can easily create undesirable large amplitude of the short waves.

Table 3. Value of ρ_m^k at t = 0 s from backward integration after 4×10^5 s (~111.1 hrs) integration.

ρ_m^k	m = 1	m = 2	m = 3	m = 4	m = 5
k = A	0.1005369673×10	$0.5492840856 \times 10^{-2}$	$-0.3766377539 \times 10^{-2}$	$-0.9312078237 \times 10^{-2}$	$-0.1152245781 \times 10^{-1}$
k = B	$-0.3693701397 \times 10^{-2}$	0.9969698423	$0.2869403506 \times 10^{-2}$	$0.6135011775 \times 10^{-2}$	$0.7802350518 \times 10^{-2}$
k = C	$0.3468797658 \times 10^{-3}$	$0.6424379574 \times 10^{-5}$	0.9995607041	$-0.8889813772 \times 10^{-3}$	$-0.1313001296 \times 10^{-2}$
k = D	$-0.2397557051 \times 10^{-4}$	$0.4867399402 \times 10^{-5}$	$-0.1797585893 \times 10^{-3}$	0.1000180041×10	$0.2610953861 \times 10^{-3}$
k = E	$0.3912165899 \times 10^{-6}$	$-0.3439648247 \times 10^{-5}$	$-0.3063946046 \times 10^{-4}$	$-0.5243916169 \times 10^{-4}$	0.1000017864×10
Total mass (M^R_0)	1.569×10^{11}	4.707×10^{11}	1.884×10^{12}	3.142×10^{12}	6.284×10^{12}
$(M^R_0 - M_{end})/M_{end}$	-1.008×10^{-3}	-5.944×10^{-4}	-2.190×10^{-4}	-1.762×10^{-6}	2.583×10^{-5}

Hence, equations of volume-integration of concentration are proposed, in which diffusion is treated as the subgrid-turbulent-fluxes across the boundaries of the cells, which depends on the turbulent velocity and density perturbation. For given turbulent velocities, the change of density of different species in each cell can be converted to a set of linear algebra equations and solved for both forward- and reverse-in time. The proposed method has been validated by the numerical simulations, which consist of 5 different sizes of concentric cylinders with different species initially. The results reveal the time evolution of compositions in each cylinder. Simulations also show that the material in each cell can change significantly during integration. The reverse integration goes through the counter-gradient diffusion process to reproduce the initial concentration of each cell, which can be very different from the downwind regions. Since the conventional forward- or backward-trajectory method ignores mixing process, it cannot be used to predict the property at the source from the downwind region, and vice versa. The method proposed here can also be applied to different cell-size, or different turbulent velocity, as long as $u'_{i,j} t_n / (V_j)^{1/3}$ is adjusted to the real environments. The results also show that the error increases as the reverse integration time increases. However, if integration time is comparable or shorter than the mixing/diffusion-time scale, the method is quite accurate.

ACKNOWLEDGES

We appreciate the reviewers for their comments. The senior author also thanks Prof. R. Nowack at Purdue University; Profs. M-C Yen, N-H Lin, C-Y Huang, P-L Lin and C. Wang at National Central University; Profs. K. Tsuboki and H. Uyeda at Nagoya University; and Prof. H. H. Hsu at Sinica Academia in Taiwan for useful discussions and helps. The computing facilities provided by Purdue University is also appreciated.

REFERENCES

Banta, R.M. (2008). Stable-boundary-layer regimes from the perspective of the low-level jet. *Acta Geophys.* 56: 58–87.

Cattaneo, C.R. (1958). Sur une forme de l'équation de la chaleur éliminant le paradoxe d'une propagation instantanée. *C.R. Acad. Sci.* 247: 431.

Chester, M. (1963). Second sound in solids. *Phys. Rev.* 131: 2013–2015.

Choi, J.C., Lee, M., Chun, Y., Kim, J. and Oh, S. (2011). Chemical composition and source signature of spring aerosol in Seoul, Korea. *J. Geophys. Res.* 106: 18067–18074.

Engl, H.W., Hanke, M. and Neubauer, A. (2000). *Regularization of Inverse Problems*. Springer Science & Business Media.

Fick, A. (1855). Uber diffusion. *Poggendorff's Ann. Phys. Chem.* 94: 59–86.

Fourier, J.B. (1822). *Théorie Analytique de la Chaleur*. Firmin-Didot père et fils, Paris, 1822. Fac simile, Ed.

Jacques Gabay, Paris 1988.

Hsu, W.R. and Sun, W.Y. (2001). A time-split, forward-backward numerical model for solving a nonhydrostatic and compressible system of equations. *Tellus Ser. A* 53: 279–299.

Lavrentiev, M.M., Romanov, V.G. and Shishatskiĭ, S.P. (1980). *Ill-posed Problems of Mathematical Physics and Analysis*. American Mathematical Society, Providence.

Medeiros, B, Hall, A. and Stevens, B. (2005). What controls the mean depth of the PBL? *J. Clim.* 18: 3157–3172.

Min, K.H. and Sun, W.Y. (2015). Atmosphere-cryosphere coupled model development and its application for regional climate studies. *Adv. Meteorol.* 2015: 764970.

Sikora, R. and Palka, I. (1980). Reverse problems for diffusion equation. *Arch. Elektrotech*. 62: 177–180.

Sun, W.Y. (1982). A comparison of two explicit time integration schemes applied to the transient heat equation. *Mon. Weather Rev.* 110: 1645–1652.

Sun, W.Y. and Chang, C.Z. (1986). Diffusion model for a convective layer: Part II: Plume released from a continuous point source. *J. Clim. Appl. Meteorol.* 25: 1454–1463.

Sun, W.Y. (1988). Air pollution in a convective atmosphere. In *Library of Environmental Control Technology*, Cheremisinoff, Ed., Gulf Publishing, pp. 515–546.

Sun, W.Y. (1989). Diffusion modeling in a convective boundary layer. *Atmos. Environ.* 23: 1205–1217.

Sun, W.Y. and Chern, J.D. (1993). Diurnal variation of lee-vortexes in Taiwan and surrounding area. *J. Atmos. Sci.* 50: 3404–3430.

Sun, W.Y, Sun, O.M.T. and Tsuboki, K. (2012). A modified atmospheric non-hydrostatic model on low aspect ratio grids. *Tellus Ser. A* 64: 17516.

Sun, W.Y., Hsu, W.R., Chern, J.D., Chen, S.H., Wu, C.C., Yang, K.J.S., Yeh, K., Bosilovich, M.G., Haines, P.A., Min, K.H., Oh, T.J., MacCall, B.T., Yildirim, A., Chang, Y.L., Chang, C.Z. and Yu, Y.C. (2012a). Purdue Atmospheric Models and Applications. In *Recent Progress in Atmospheric Sciences: Applications to the Asia-Pacific Region*. Liou, K.N. and Chou, M.D. (Eds.), World Scientific Publishing, Singapore, pp. 200–230.

Sun, W.Y., Yang, K.J.S. and Lin, N.H. (2013a). Numerical simulations of Asian dust aerosols and regional impacts on weather and climate- Part I: Control Case-PRCM simulation without dust-aerosols. *Aerosol Air Qual. Res.* 13: 1630–1640.

Sun, W.Y., Yang, K.J.S. and Lin, N.H. (2013b). Numerical simulations of Asian dust aerosols and regional impacts on weather and climate- Part II: PRCM-Dust model simulation. *Aerosol Air Qual. Res.* 13: 1641–1654.

Sun, W.Y, Sun, O.M. and Tsuboki, K. (2013c). A modified atmospheric non-hydrostatic model on low aspect ratio grids: Part II. *Tellus Ser. A* 65: 19681.

Sun, W.Y. and Sun, O.M. (2015). Bernoulli equation and flow over a mountain. *Geosci. Lett.* 2: 7.

Taitel, Y. (1971). On the parabolic, hyperbolic and discrete formulation of the heat conduction equation. *Int. J. Heat Mass Transfer* 15: 369–371.

Tsuboki, K. and Sakakibara, A. (2007). *The Seventeenth IHP Training Course* (International Hydrological Program). Numerical Prediction of High-Impact Weather Systems, 2 15 December 2007, Nagoya, Japan.

Vernotte, P. (1958). Les paradoxes de la theorie continue de l'équation de la chaleur. *C.R. Acad. Sci.* 246: 3154.

Yang, K.J.S. (2004). *Regional climate-chemistry model simulations of Ozone in the lower troposphere and its climatic impacts*. Ph.D. Thesis, School of Civil Engineering, Purdue Univ., W. Lafayette, IN 47907.

Received for review, June 28, 2016
Revised, October 30, 2016
Accepted, October 31, 2016